

Quantifying the role of ocean coupling in Arctic amplification and sea-ice loss over the 21st century

Rei Chemke¹, Lorenzo M. Polvani^{2,3}, Jennifer E. Kay⁴ & Clara Orbe^{2,5}

¹*Department of Earth and Planetary Sciences, Weizmann Institute of Science, Rehovot, Israel*

²*Department of Applied Physics and Applied Mathematics, Columbia University, New York, NY, USA*

³*Department of Earth and Environmental Sciences, and Lamont-Doherty Earth Observatory, Columbia University, Palisades, NY 10964, USA*

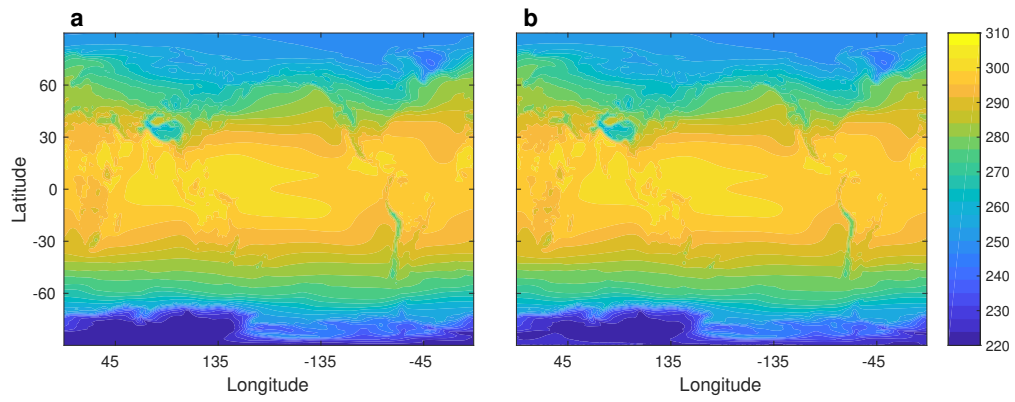
⁴*Cooperative Institute for Research in Environmental Sciences, and Department of Atmospheric and Oceanic Sciences, University of Colorado Boulder, Boulder, Colorado, USA*

⁵*NASA Goddard Institute for Space Studies, New York, NY, 10025 USA*

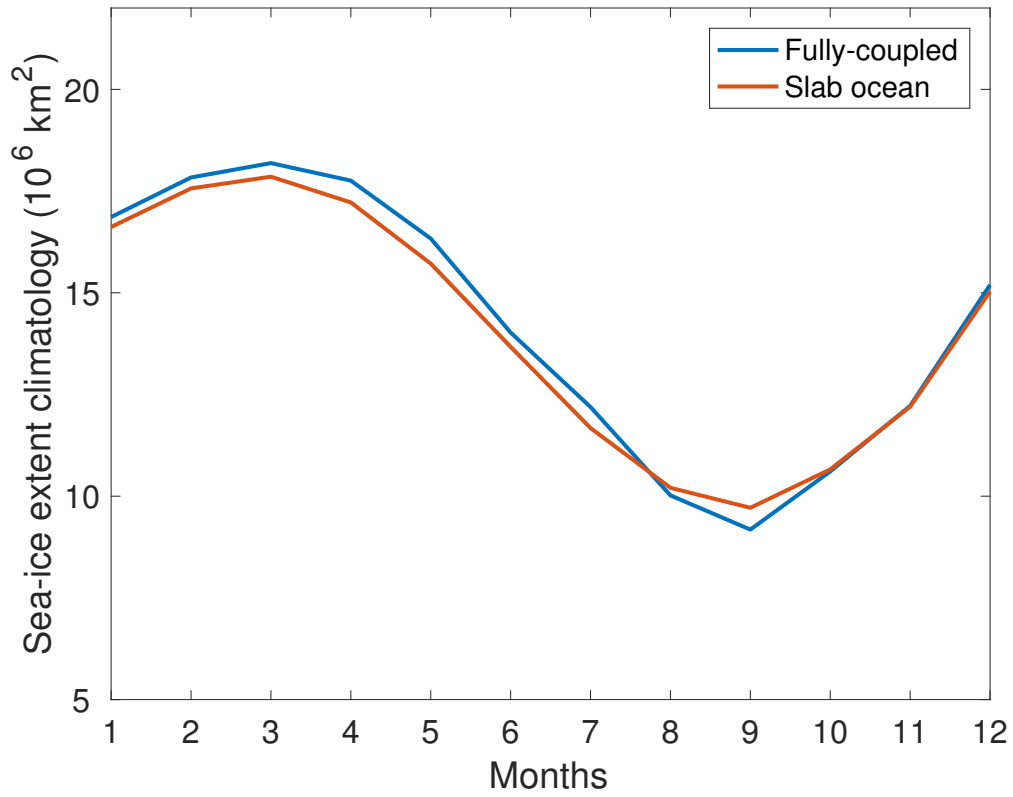
Table 1: List of the 38 CMIP5 models analyzed in this study.

	Model	Modeling Center
1	ACCESS1.0	CSIRO (Commonwealth Scientific and Industrial Research Organisation, Australia), and BOM (Bureau of Meteorology, Australia)
2	ACCESS1.3	CSIRO (Commonwealth Scientific and Industrial Research Organisation, Australia), and BOM (Bureau of Meteorology, Australia)
3	bcc-csm1-1	Beijing Climate Center, China Meteorological Administration
4	bcc-csm1-1-m	Beijing Climate Center, China Meteorological Administration
5	BNU-ESM	College of Global Change and Earth System Science, Beijing Normal University
6	CanESM2	Canadian Centre for Climate Modelling and Analysis
7	CCSM4	National Center for Atmospheric Research
8	CESM1-BGC	National Science Foundation, Department of Energy, National Center for Atmospheric Research
9	CESM1-CAM5	National Science Foundation, Department of Energy, National Center for Atmospheric Research
10	CMCC-CESM	Centro Euro-Mediterraneo per I Cambiamenti Climatici
11	CMCC-CM	Centro Euro-Mediterraneo per I Cambiamenti Climatici
12	CMCC-CMS	Centro Euro-Mediterraneo per I Cambiamenti Climatici
13	CNRM-CM5	Centre National de Recherches Meteorologiques / Centre Europeen de Recherche et Formation Avancees en Calcul Scientifique
14	CSIRO-Mk3-6-0	Commonwealth Scientific and Industrial Research Organisation in collaboration with the Queensland Climate Change Centre of Excellence
15	FGOALS-g2	LASG, Institute of Atmospheric Physics, Chinese Academy of Sciences; and CESS, Tsinghua University
16	FGOALS-s2	LASG, Institute of Atmospheric Physics, Chinese Academy of Sciences; and CESS, Tsinghua University
17	FIO-ESM	The First Institute of Oceanography, SOA, China
18	GFDL-CM3	Geophysical Fluid Dynamics Laboratory
19	GFDL-ESM2G	Geophysical Fluid Dynamics Laboratory
20	GFDL-ESM2M	Geophysical Fluid Dynamics Laboratory
21	GISS-E2-H	NASA Goddard Institute for Space Studies
22	GISS-E2-H-CC	NASA Goddard Institute for Space Studies
23	GISS-E2-R	NASA Goddard Institute for Space Studies
24	GISS-E2-R-CC	NASA Goddard Institute for Space Studies
25	HadGEM2-AO	Met Office Hadley Centre (additional HadGEM2-ES realizations contributed by Instituto Nacional de Pesquisas Espaciais)
26	HadGEM2-CC	Met Office Hadley Centre (additional HadGEM2-ES realizations contributed by Instituto Nacional de Pesquisas Espaciais)

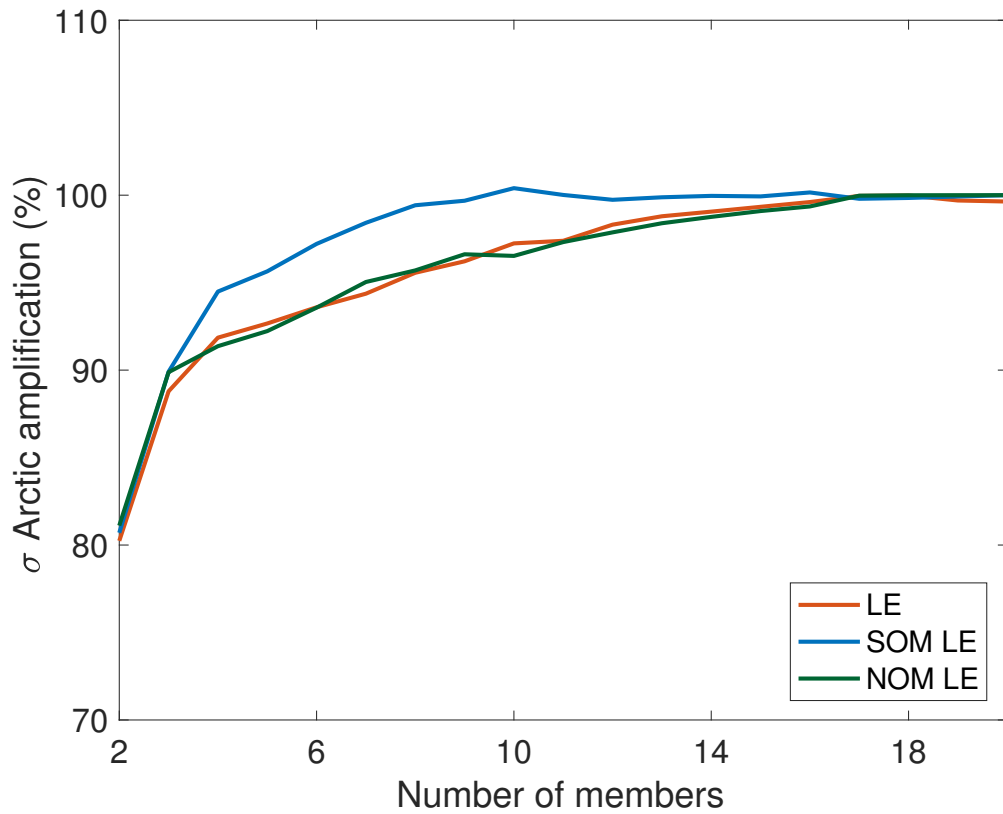
27	HadGEM2-ES	Met Office Hadley Centre (additional HadGEM2-ES realizations contributed by Instituto Nacional de Pesquisas Espaciais)
28	INMCM4	Institute for Numerical Mathematics
29	IPSL-CM5A-LR	Institut Pierre-Simon Laplace
30	IPSL-CM5A-MR	Institut Pierre-Simon Laplace
31	IPSL-CM5B-LR	Institut Pierre-Simon Laplace
32	MIROC5	Atmosphere and Ocean Research Institute (The University of Tokyo), National Institute for Environmental Studies, and Japan Agency for Marine-Earth Science and Technology
33	MIROC-ESM	Japan Agency for Marine-Earth Science and Technology, Atmosphere and Ocean Research Institute (The University of Tokyo), and National Institute for Environmental Studies
34	MIROC-ESM-CHEM	Japan Agency for Marine-Earth Science and Technology, Atmosphere and Ocean Research Institute (The University of Tokyo), and National Institute for Environmental Studies
35	MPI-ESM-LR	Max Planck Institute for Meteorology (MPI-M)
36	MPI-ESM-MR	Max Planck Institute for Meteorology (MPI-M)
37	MRI-CGCM3	Meteorological Research Institute
38	NorESM1-M	Norwegian Climate Centre



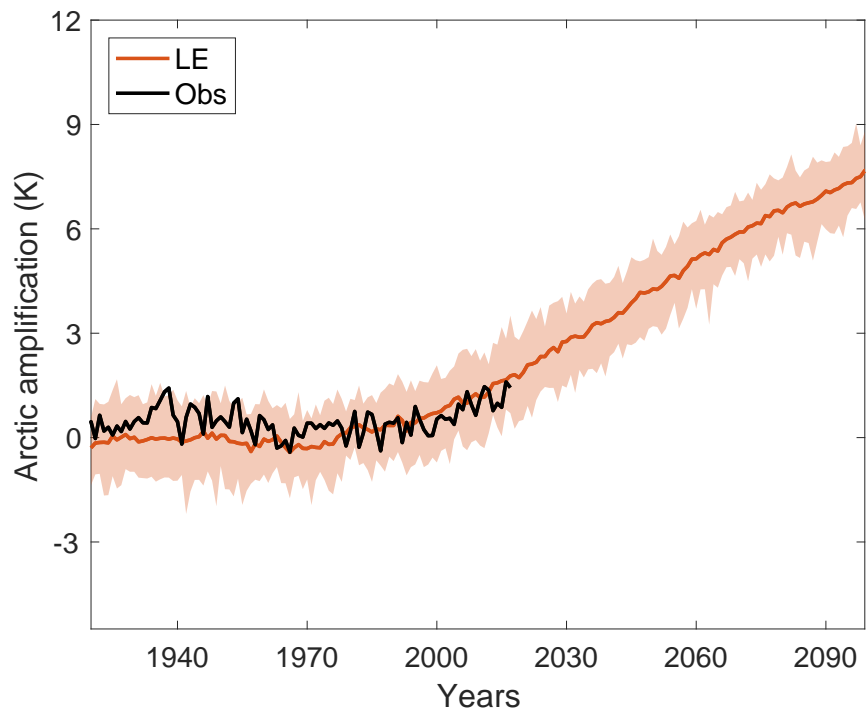
Supplementary Fig. 1. Preindustrial climatology of near-surface air temperature (SAT) in (a) fully coupled and (b) slab ocean models of the CESM1.



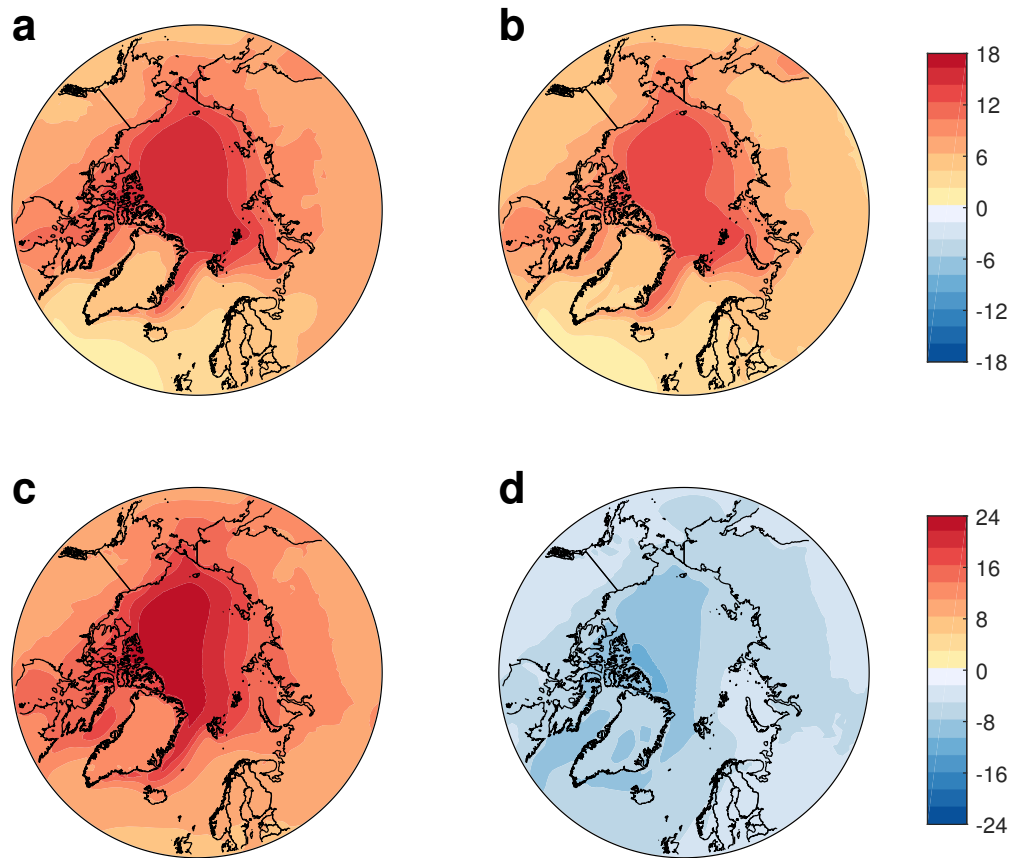
Supplementary Fig. 2. Preindustrial climatological monthly Arctic sea-ice extent (10^6 km^2) for the fully coupled (red) and slab ocean (blue) configurations of the CESM1.



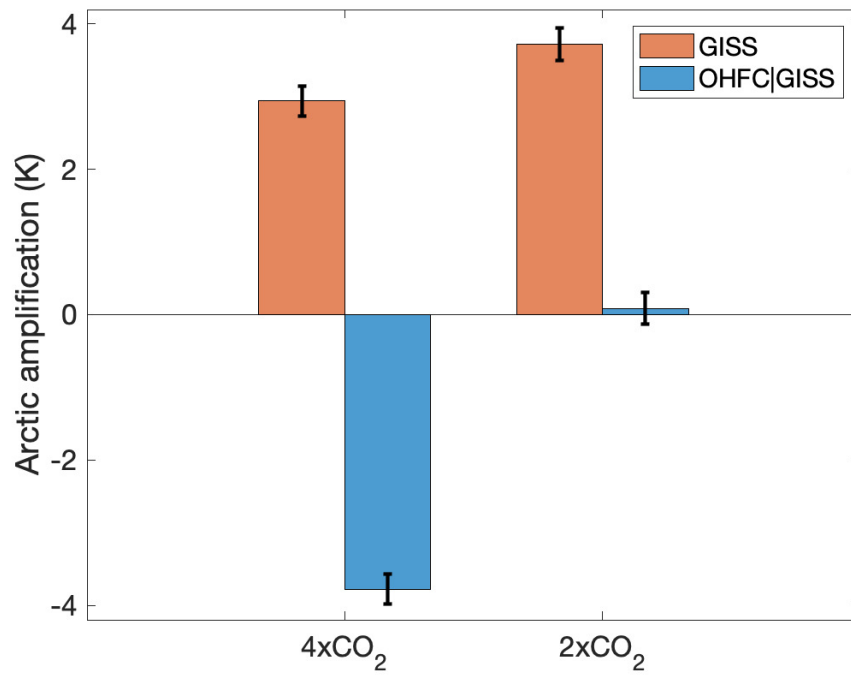
Supplementary Fig. 3. One standard deviation of Arctic amplification, across different number of ensemble members, relative to one standard deviation across all members. The standard deviation is calculated each year, and averaged over the 20th and 21st centuries, and over all combinations of number of ensemble members (or up to 1000 random combinations) in LE (red), SOM LE (blue) and NOM LE (green).



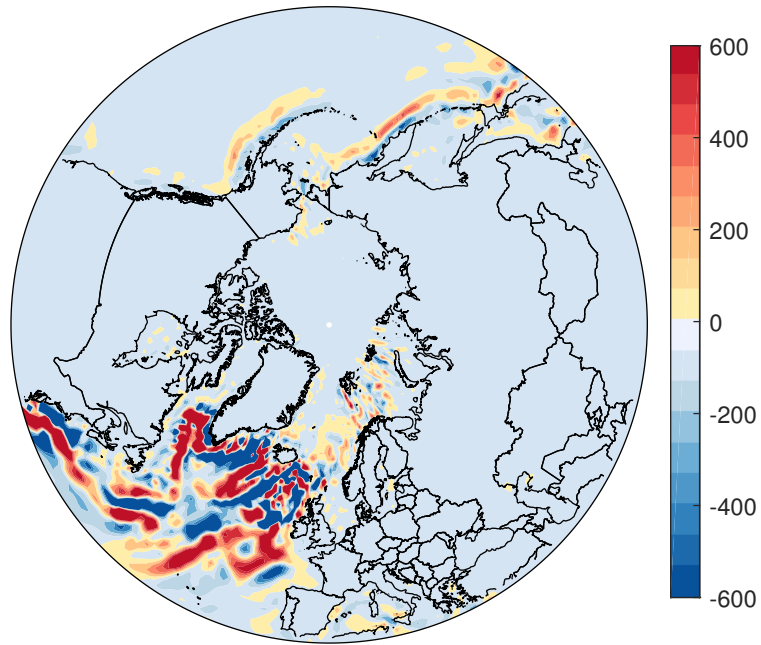
Supplementary Fig. 4. Evolution of Arctic amplification for the LE mean (red line), and the observations (black line, HadCRUT4). The Amplification is here defined relative to the 1961-1990 period, for consistency with the HadCRUT4 data set.



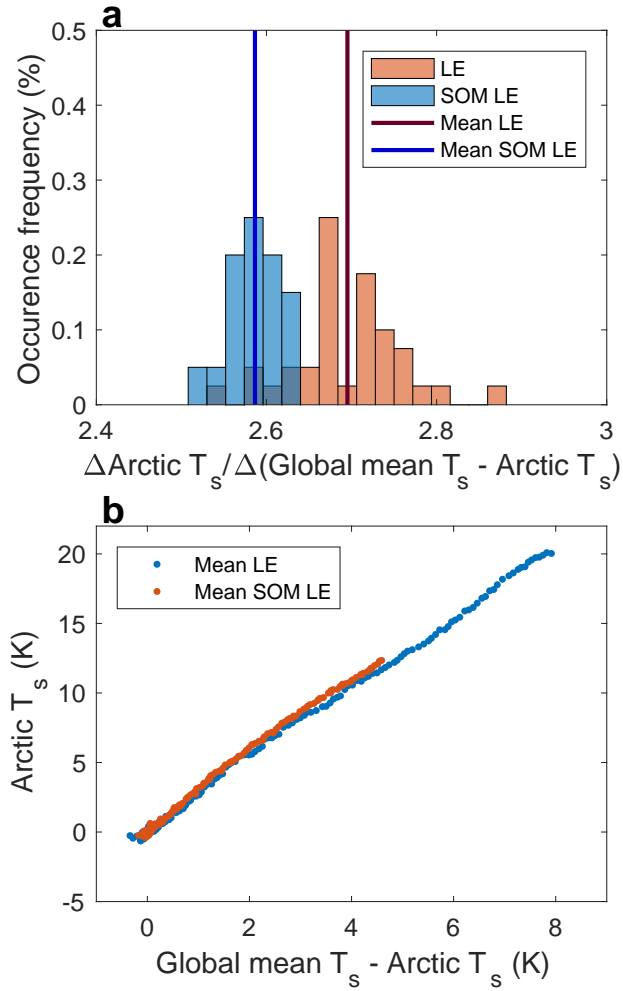
Supplementary Fig. 5. Response (differences between the 2080-2099 and 1980-1999 periods) of the near-surface air temperature (K) in a, the LE mean, and the contribution from b, net ocean coupling, c, thermodynamic coupling and d, dynamic coupling. The (very few) small black dots show where the differences are not statistically significant at the 95% confidence level.



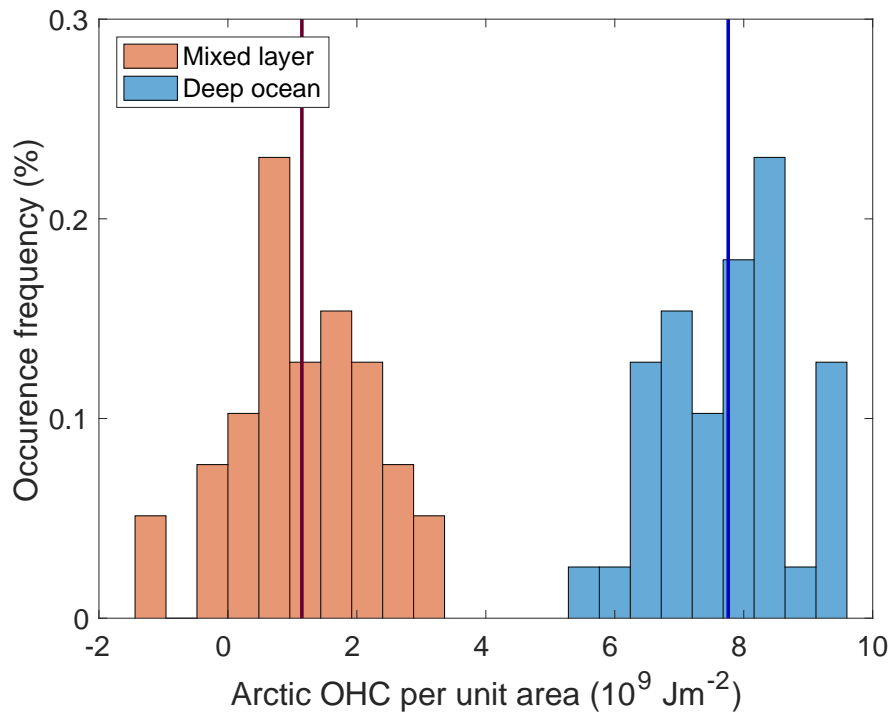
Supplementary Fig. 6. Arctic amplification (K), relative to preindustrial values, in response to quadrupling (left) and doubling (right) CO₂ concentrations in GISS Model E2.1. Red and blue bars show the amplification in the fully-coupled configuration and the contribution of OHFC, respectively. Error bars represent the 95% confidence interval.



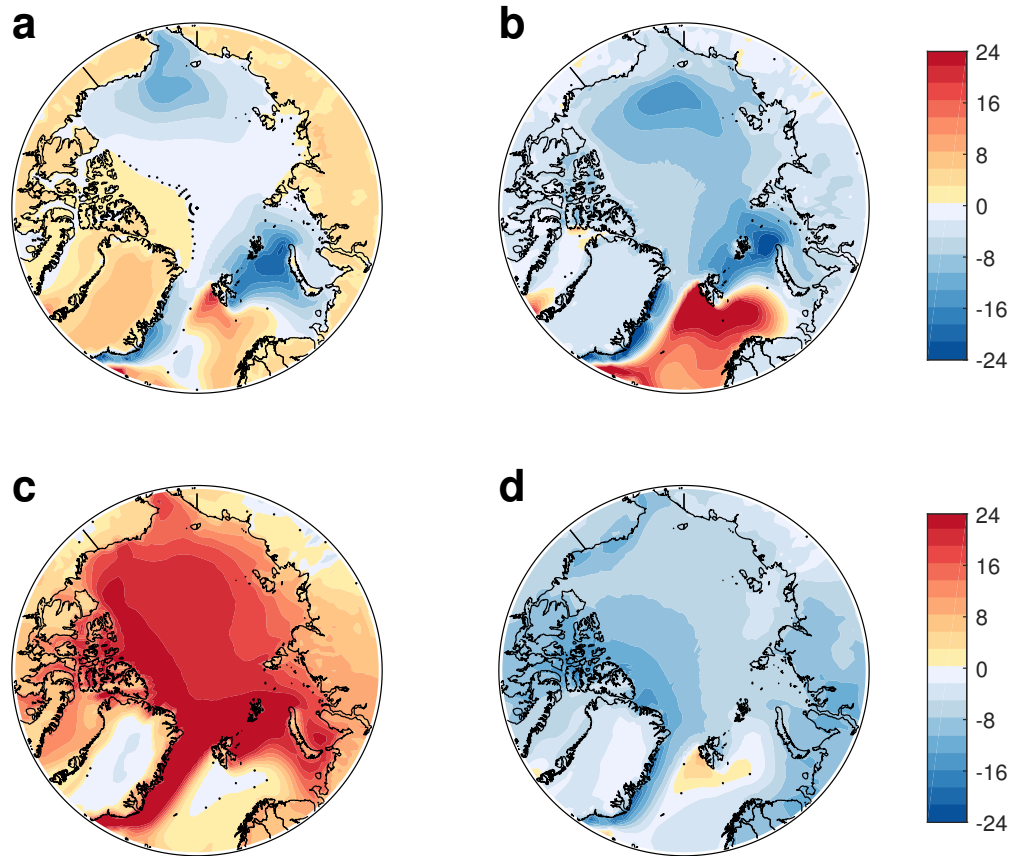
Supplementary Fig. 7. Response (differences between the 2080-2099 and 1980-1999 periods) of the mixed-layer meridional heat flux convergence (Wm^{-2}). The (very few) small black dots show where the differences are not statistically significant at the 95% confidence level.



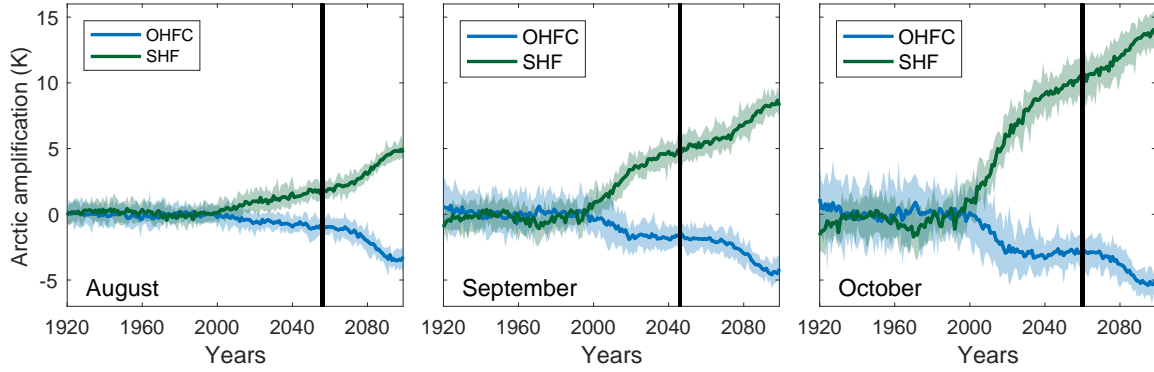
Supplementary Fig. 8. (a) The occurrence frequency (in percentage) of the projected (over the 2080-2099 period) Arctic amplification, defined as the ratio between the warming of near-surface air temperature in the Arctic and the warming over rest of the world, in LE (red bars) and SOM LE (blue bars). The red and blue vertical lines show the amplification for LE mean and SOM LE mean, respectively. (b) Arctic near-surface air temperature anomalies, relative to the 1980-1999 period, as a function of the rest of the world near-surface air temperature anomalies in LE mean (red dots) and SOM LE mean (blue dots).



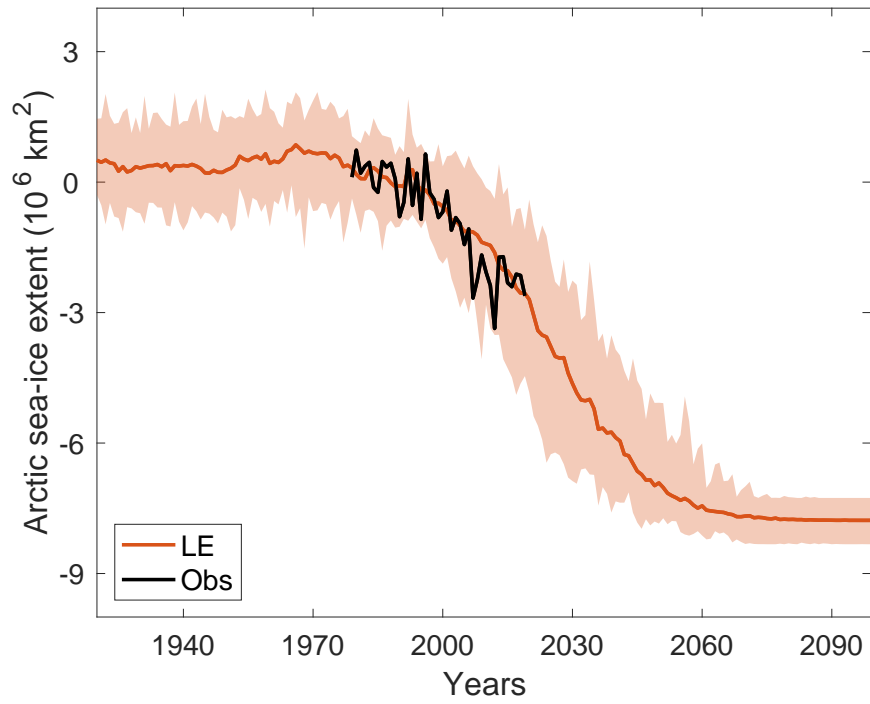
Supplementary Fig. 9. The occurrence frequency (in percentage) of the response (differences between the 2080-2099 and the 1980-1999 periods) of subsurface Arctic ocean heat content (OHC), per unit area (10^9 Jm^{-2}), in the mixed layer (red) and deep ocean (blue). The red and blue vertical lines show the response for the ensemble mean.



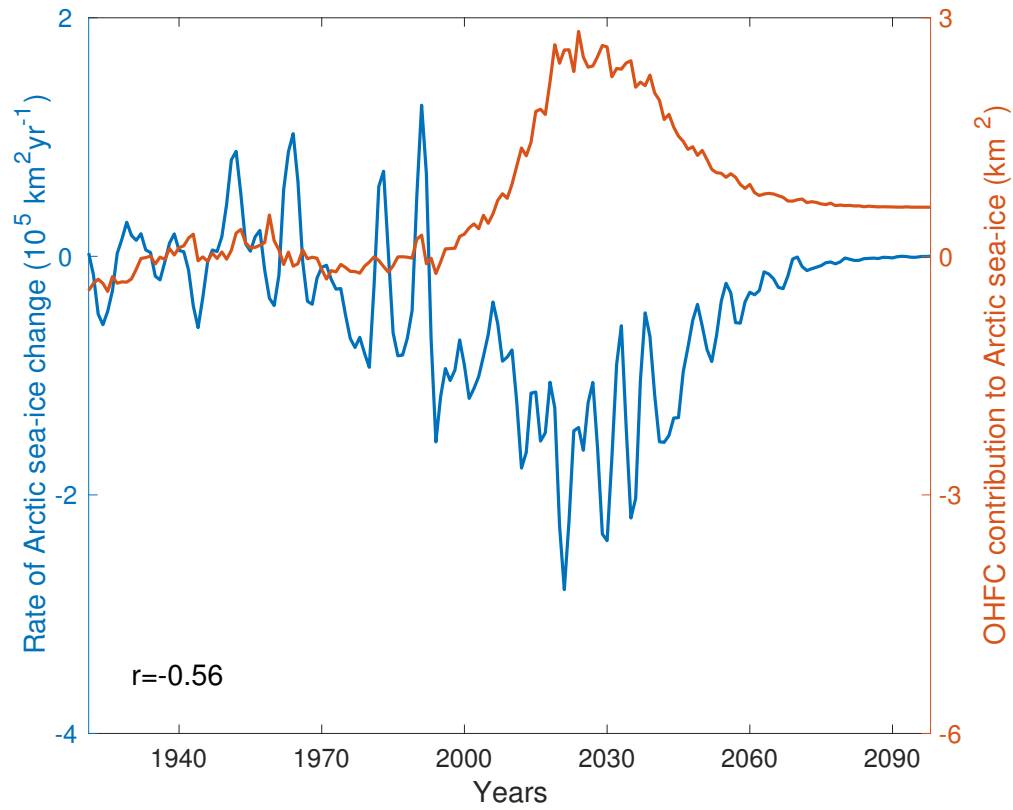
Supplementary Fig. 10. The difference between the response of surface heat fluxes (Wm^{-2}) over the Arctic ($66^\circ\text{N} - 90^\circ\text{N}$), and over the rest of the Earth; a, latent heat fluxes b, sensible heat fluxes, c, shortwave radiation and d, longwave radiation. The (very few) small black dots show where the differences are not statistically significant at the 95% confidence level.



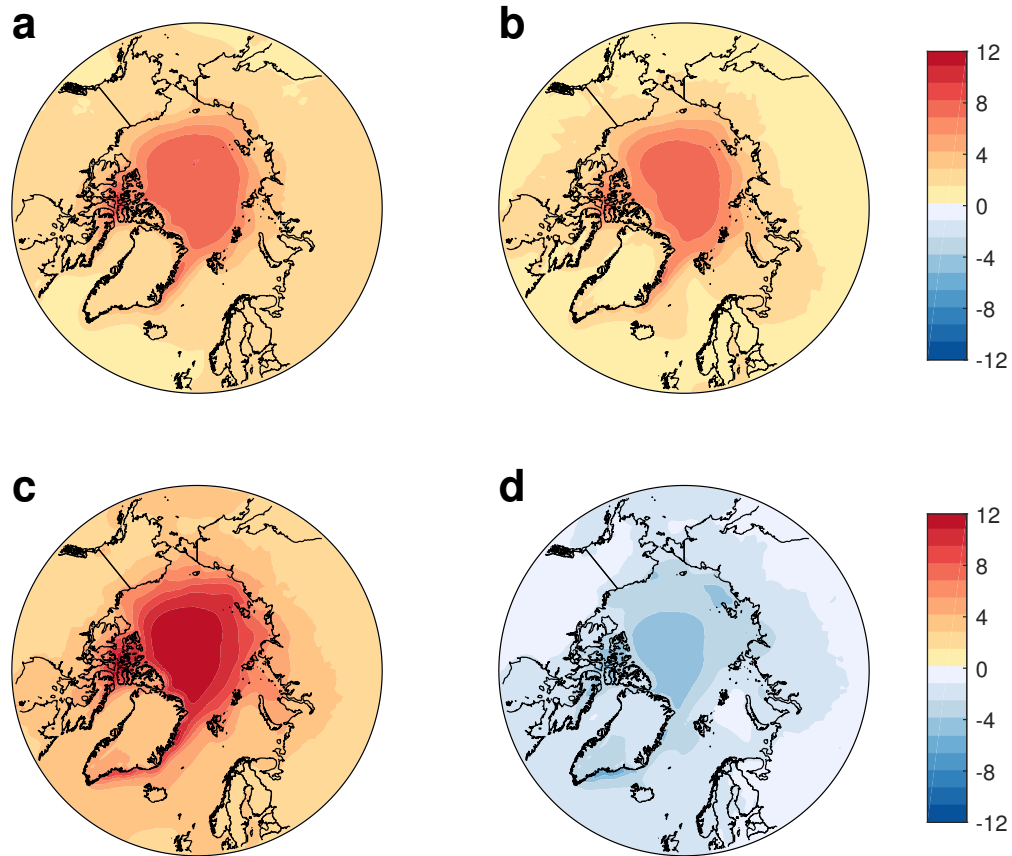
Supplementary Fig. 11. Evolution of the contribution of dynamic (OHFC, blue) and thermodynamic (SHF, green) ocean coupling to Arctic amplification in August (left), September (middle) and October (right). The vertical black lines represent the year of ice-free conditions (sea-ice extent $\leq 10^6 \text{ km}^2$).



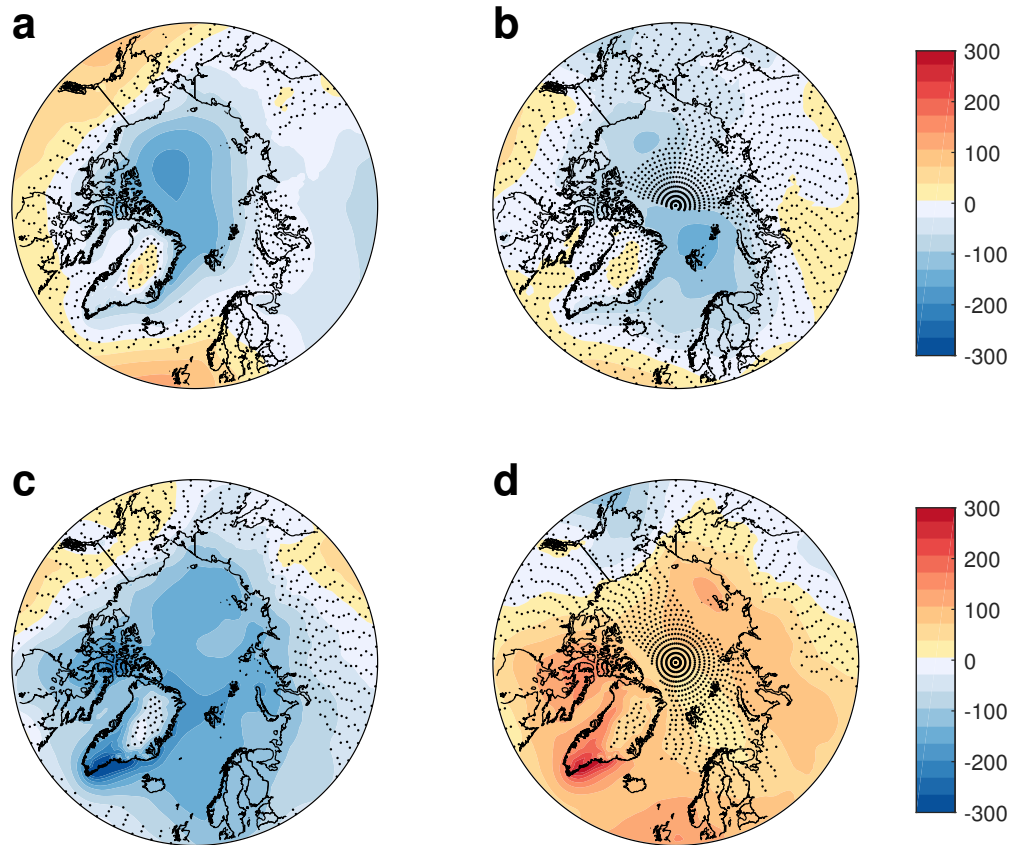
Supplementary Fig. 12. Time series, relative to the 1980-1999 periods, of September Arctic sea-ice extent for the LE mean (red line), and the observations (black line, NSIDC).



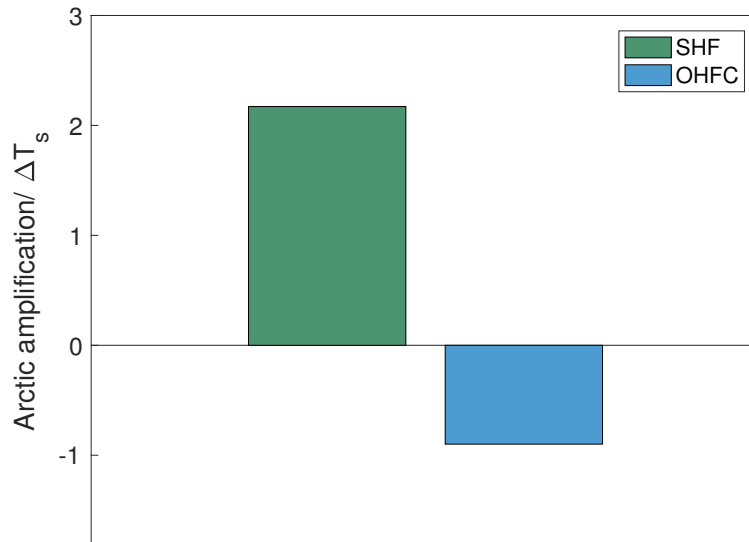
Supplementary Fig. 13. Time evolution of the rate of Arctic sea-ice change (blue, $10^5 \text{ km}^2 \text{ yr}^{-1}$) and the contribution from dynamic coupling (OHFC) to changes in Arctic sea-ice (red, km^2). Both lines show the mean of the ensembles, and their correlation is shown in the lower left corner.



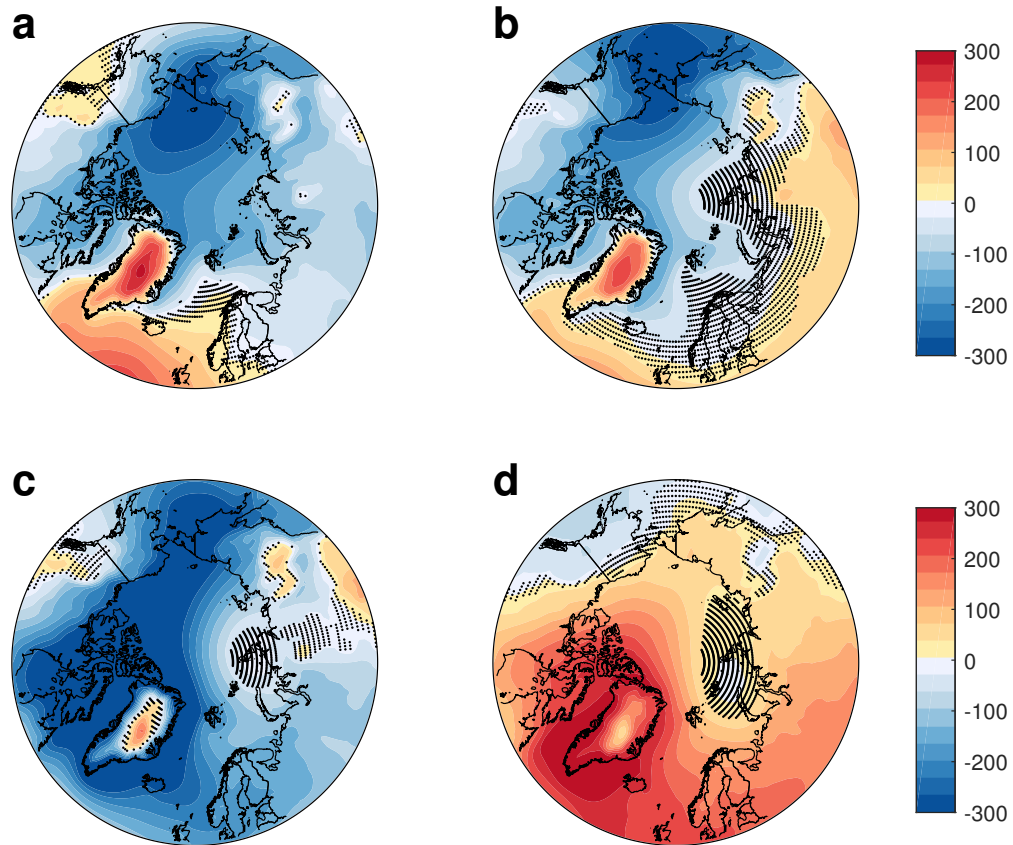
Supplementary Fig. 14. Response (differences between the 2020-2040 and 1980-1999 periods) of September near-surface air temperature (K) in a, the LE mean, and the contribution from b, net ocean coupling, c, thermodynamic coupling and d, dynamic coupling. The (very few) small black dots show where the differences are not statistically significant at the 95% confidence level.



Supplementary Fig. 15. Response (differences between the 2020-2040 and 1980-1999 periods) of September sea level pressure (Pa) in a, the LE mean, and the contribution from b, net ocean coupling, c, thermodynamic coupling and d, dynamic coupling. The small black dots show where the differences are not statistically significant at the 95% confidence level.



Supplementary Fig. 16. Sensitivity to surface temperature changes of the roles of thermodynamic (green) and dynamic (blue) ocean coupling in Arctic amplification over the 21st century, estimated by calculating the linear trends of SHF and OHFC as a function of global mean surface temperature over the 21st century.



Supplementary Fig. 17. Response (differences between the 2080-2099 and 1980-1999 periods) of the annual mean sea level pressure (Pa) in a, the LE mean, and the contribution from b, net ocean coupling, c, thermodynamic coupling and d, dynamic coupling. The small black dots show where the differences are not statistically significant at the 95% confidence level.